Instability and Transition in Shock-Induced Separation Bubbles

Alessandro Pagella, Ulrich Rist
Universität Stuttgart
Institut für Aerodynamik und Gasdynamik
Pfaffenwaldring 21, 70550 Stuttgart, Germany

rist@iag.uni-stuttgart.de

ABSTRACT

In the present work, a flow field with a free-stream Mach number Ma=6 is computed, where an oblique shock entering the integration domain from the free stream hits a two-dimensional laminar boundary layer causing a laminar separation bubble. Then the instability of the flow with respect to small-amplitude two- and three-dimensional disturbance waves is investigated using linear stability theory (LST) and direct numerical simulations (DNS). In order to get an idea about the contributions of non-linear disturbances different scenarios with large-amplitude forcing are compared to each other, and their effect on the mean-flow is discussed. In all investigated cases the transition mechanism is found to provide initial amplitudes for an ensuing Görtler-type instability in the reattaching boundary layer which then grow irrespective of their origin.

1.0 INTRODUCTION

Laminar-turbulent transition in super- and hypersonic boundary layers does not only have strong influence on wall-shear stresses and heat flux, but also on other flow phenomena like shock-wave/boundary-layer interaction and flow separation, and can therefore influence the global flow field and the aerodynamic drag substantially. Shock-wave/boundary-layer interaction itself is one major area of concern in technical applications at hypersonic speeds. It can result in high aerodynamic loads, engine inlet performance loss and increase of drag, to name only a few examples [1], [4]. For air-breathing propulsion systems of the lower stage of space vehicles a thin laminar boundary layer on the fore body, designed to compress the air before the flow enters the engine intake, is clearly favourable.

Direct Numerical Simulations (DNS) of high-order accuracy and resolution performed on supercomputers can enable new and deep insights into fundamental small-scale or high-frequency flow phenomena like the transition process. An example is the simulation of the physically unstable, dynamical processes during laminar-turbulent transition in a shock-induced laminar separation bubble. However, in order to control the process for a better study of its mechanisms and a better understanding, it is necessary to trigger laminar-turbulent transition by a well-defined disturbance input. This mimics so-called controlled experiments where the background disturbance level of the experimental facility is extremely low and special disturbance devices are used.

2.0 NUMERICAL METHOD

The simulations presented here allow the investigation of the spatial instability and the laminar-turbulent transition of supersonic boundary-layer flows along a flat plate or a sharp cone, respectively. Time-wise periodic two- and three-dimensional disturbance waves with defined frequency and amplitude are triggered in a two-dimensional, laminar and steady-state base flow. The reactions of the base flow to these disturbances, i.e. the downstream evolution of the excited disturbance waves, is simulated within the integration domain by numerical solution of the complete, three-dimensional, unsteady, compressible Navier-Stokes equations supplemented by the continuity and energy equation:

$$\frac{\partial \rho}{\partial t} + \nabla \cdot \left(\rho \vec{u} \right) = 0 \tag{1}$$

$$\frac{\partial \left(\rho \vec{u} \right)}{\partial t} + \nabla \cdot \left(\rho \vec{u} \vec{u} \right) + \nabla p = \frac{1}{\mathrm{Re}} \nabla \vec{\sigma} \tag{2}$$

$$\frac{\partial (\rho e)}{\partial t} + \nabla \cdot (p + \rho e)\vec{u} = \frac{1}{(\kappa - 1)\mathrm{Re}\,\mathrm{Pr}\,Ma^2} \nabla \cdot (\vartheta \nabla T) + \frac{1}{\mathrm{Re}} \nabla \cdot \left(\vec{\sigma} \vec{u} \right), \tag{3}$$

where $\vec{u} = (u, v, w)^T$, and

$$\vec{\sigma} = \mu \left[\left(\nabla \vec{u} + \nabla \vec{u}^T \right) - \frac{2}{3} \left(\nabla \cdot \vec{u} \right) I \right] \tag{4}$$

is the viscous stress and

$$e = \int c_v(T)dT + \frac{1}{2} \left(u^2 + v^2 + w^2 \right) \tag{5}$$

is the internal energy per mass unit. The fluid is considered as a non-reacting, perfect gas, for which the equation of state

$$p = \frac{1}{\kappa_\infty Ma_\infty^2} \cdot \rho T \tag{6}$$

is valid. The thermodynamic properties of the fluid are approximated as a *calorically perfect gas* with specific heats c_P, c_V and a Prandtl number *Pr=0.71* which are assumed constant with the specific heat ratio $\kappa = c_P/c_V = 1.4$. For temperatures above the Sutherland temperature $T_s = 110.4\ K$ the dynamic viscosity μ is determined from Sutherland's law and the thermal conductivity ϑ is set proportional to the viscosity. For lower temperatures μ is set proportional to *T*.

In the following, lengths are non-dimensionalized by a reference length *L*, which appears in a global Reynolds number $Re=\rho_\infty \cdot u_\infty \cdot L/\mu_\infty = 10^5$. A second Reynolds number used here is $R_x = \sqrt{x \cdot \mathrm{Re}}$. Time *t* is normalized by L/u_∞. The specific heat c_V is normalized with u^2_∞/T_∞. Flow quantities with subscript ∞ denote free-stream values. Density, temperature and viscosity are also non-dimensionalized with their respective free-stream values.

We assume a numerical grid with $N \cdot M$ grid points in streamwise (*x*) and wall-normal direction (*y*), as well as *K* harmonics in spanwise direction (*z*). In streamwise direction the solution has a wave character in the presence of disturbance waves, which are either amplified or damped. Compact finite differences are able to resolve this kind of solution in an appropriate manner. They are applied here in a split-type form [8]. This form has some damping characteristics with respect to small-scale oscillations. In wall-normal direction standard finite differences of fourth-order accuracy are used. Split-type differences are used to calculate convective terms, while viscous terms are computed by central differences. In spanwise direction periodic boundaries allow a spectral approximation with Fourier expansion. Time integration is performed with a standard 4-step Runge-Kutta scheme of fourth-order accuracy.

The numerical simulation starts with computing a laminar base flow which satisfies the basic equations in steady, two-dimensional form, using pseudo time-stepping for integrating the time-dependent equations to a steady state. This base flow constitutes the initial condition for the disturbance calculation at *t=0*. Then, for *t>0*, disturbances are introduced, and the real-time downstream development of the disturbance waves is calculated solving the full equations. For this purpose the method of disturbance flow formulation is used, i.e. each flow quantity is decomposed into its base flow and disturbance part ($\phi = \phi_B + \phi'$). It is assumed that there is no alteration of the base flow in time. Note that any change of the time-mean of the flow is represented by $\langle \phi' \rangle \neq 0$, thus there is no linearization.

The inflow variables result from calculations of the compressible boundary layer equations [1], [5] and are held constant during simulation, i.e. disturbances are zero at the inflow boundary for all time. At the outflow boundary, base-flow field variables are calculated neglecting second streamwise derivatives. Disturbance values are treated using a buffer domain [9] where all values are smoothly damped to zero in order to avoid reflections from the boundary.

At the wall, the no-slip condition and vanishing normal velocity component are assumed. Disturbances are introduced within a disturbance strip located at the wall by varying the wall-normal momentum disturbance *(ρv)'* simulating periodic blowing and suction. A thorough description of the disturbance function applied can be found in [5] and [12]. The wall-temperature can be modeled as constant ($T_B = const$, *T' = 0*), adiabatic ($\partial T/\partial y=0$) or radiation-adiabatic (see [5]).

At the free-stream boundary, the shock is prescribed using flow variables computed form the Rankine-Hugoniot relations for a chosen shock angle. Thus, for several grid-points up- and downstream of the shock the flow variables are held constant. For the remaining boundary points a characteristic boundary condition [5] is applied for the base flow calculation. As a result, a steady shock establishes itself within the flow field during calculation of the base flow (see next section).

For the disturbance calculations, a non-reflecting boundary condition according to [15] is used at the free-stream boundary. For a more thorough description of the numerical scheme see [5]. All simulations have been performed on the supercomputers NEC SX-4 and SX-5 of the high performance computing center Stuttgart, HLRS, which are perfectly capable of dealing with the complex and challenging computations.

3.0   RESULTS

3.1   Base Flow Properties

In the following, laminar boundary layers at a free-stream Mach number *Ma = 6.0*, free stream temperature $T_\infty = 78\ K$ and two different wall-boundary conditions are considered: an isothermal one where the wall temperature is held constant at $T_w = 300\ K$, and the adiabatic condition, respectively. In the latter case the wall temperature establishes itself between *547* and *560 K*. Thus, compared to the adiabatic case, the isothermal wall is cooler. Later, this will have some consequences on the instability of the boundary layer. The oblique shock enters the domain through the free-stream boundary at an angle with respect to the wall of $\sigma = 12^o$.

The density field for the case with adiabatic wall is shown in Fig. 1 together with some selected streamlines in the central region of the flow field. The latter visualize the flow directions in the free stream and inside the boundary layer, where a rather large separation bubble can be observed. The pressure gradient of the impinging shock thickens the boundary layer such that, due to the displacement of the flow, compression waves are formed up- and downstream of shock-impingement. Provided the shock is strong enough, the boundary layer separates. Further away from the boundary layer, the compression waves near separation and reattachment will merge into the separation- and reattachment-shock, respectively, but this region lies outside of the present domain. On its way into the boundary layer, the impinging oblique shock steepens until it reaches the sonic line from where it reflects as an expansion fan.
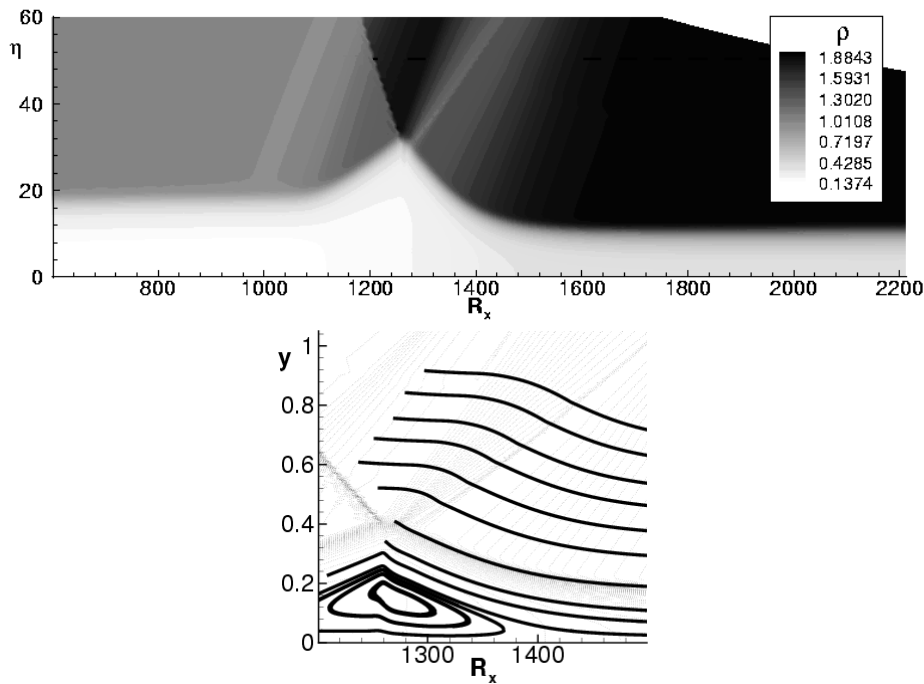
Figure 1: Density field (top) and streamlines (bottom) of the base flow. $R_x = (100000\ x)^{1/2}$. Note: the angle of the impinging shock with respect to the horizontal is $\sigma = 12^o$

In Fig. 2 the skin friction coefficients for both cases with different wall boundary conditions are compared to each other. Separation and reattachment are characterized by zero wall friction and inside the separation bubble the wall friction is negative. The separation bubble of the adiabatic case turns out to be twice as large as in the wall-cooling case. Additional simulations with halved step-sizes in x or y direction prove the grid-independence of these results.
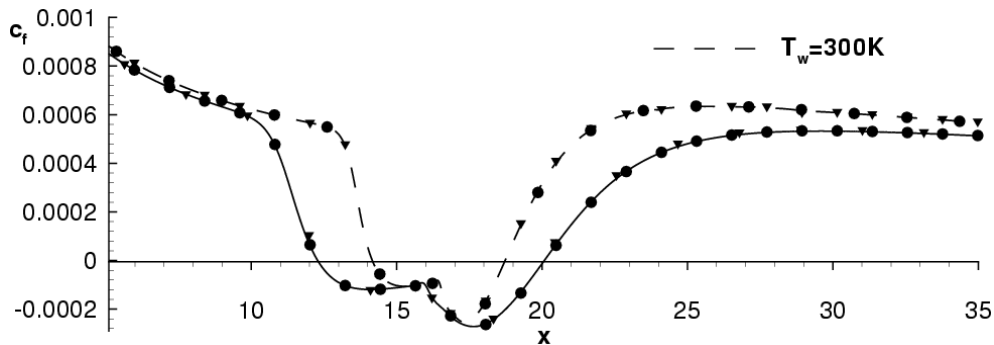
Figure 2: Comparison of skin friction coefficients for the computations with constant wall temperature (— —) and adiabatic wall boundary condition (——)

The different wall-pressure distributions are compared in Fig. 3 confirming the wall-temperature dependent bubble lengths. The pressure rise imposed by the shock splits into an 'upstream' and a 'downstream' region (relative to shock impingement), a typical feature of shock/boundary-layer interaction. Downstream of the interaction zone the wall pressure remains somewhat lower in the adiabatic case.
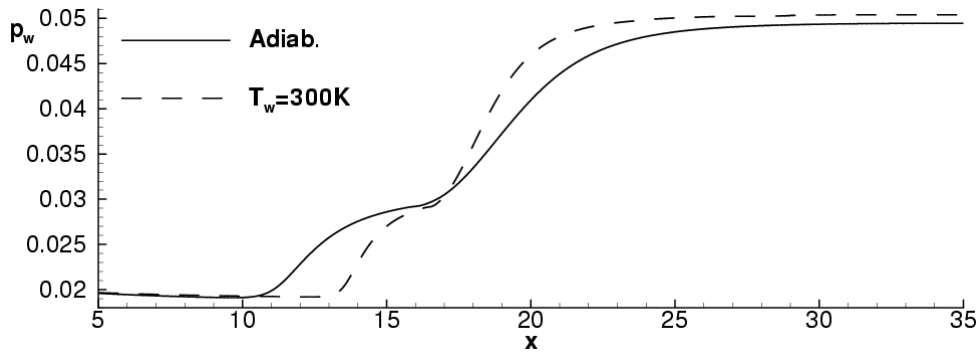
Figure 3: Comparison of wall pressures for the computations with constant wall temperature and adiabatic wall boundary condition

Although the base flow properties have been intensively studied, much less is known about the transitional behavior of such flows with shock-wave/boundary-layer interaction. Transition to turbulence is of high significance in practical hypersonic flows. Depending on the flight state, the transition zone can have a comparable length with respect to the fully turbulent flow on the body of a vessel [1]. Also, temperature disturbance peaks can reach even higher values than in turbulent flow, which has to be considered in structural design. Therefore, we will investigate the instability and amplification with respect to small-amplitude disturbances in the next section.

3.2   Small-Amplitude Disturbance Behavior

We now compare compressible linear stability theory results (for two-dimensional disturbances only) obtained from investigations of both above base-flow configurations first without, then with the impinging shock. Our linear stability theory results are based on the scheme developed by Mack [7]. Non-parallel base-flow effects are not taken into account here. The stream-wise velocity and temperature profiles, which are used by linear stability theory, were extracted locally from the direct numerical simulations of the base flow. Figure 4 compares the stability diagrams of the hypersonic boundary layers without shock impingement but otherwise the same boundary conditions as specified above. The normalized frequency *F* is defined by

$$F = (2 \cdot \pi \cdot f^* \cdot L)/(u^*_\infty \cdot Re), \tag{7}$$

and the amplification rates by

$$\alpha_i = (-\partial \ln(A(x)/A_0))/\partial x, \tag{8}$$

where $A(x)/A_0$ refers to an amplitude ratio with respect to an initial amplitude of an arbitrary flow variable. The dimensional disturbance frequency is denoted by f^*. All variables with an asterisk * and the reference length L are dimensional.

As it can be seen, the cooled wall ($T_w = 300\ K$) has a narrower domain of instability (with respect to frequency) but considerably larger amplification rates. The according disturbances are of the so-called second mode kind (according to Mack [7]). Hence the instability region at low frequencies in the adiabatic case belongs to the first mode, whose according three-dimensional disturbances are more amplified than the two-dimensional ones in the present figure. Changes due to the impinging shock become apparent in Fig. 5. Darker gray levels in comparison with the previous figure indicate that the amplification rates have increased. However, the influence of the oblique shock on the stability diagrams is rather local. For instance, the first-mode instability is completely suppressed in the region of shock/boundary-layer interaction in the adiabatic case. Two other apparent features are the shift of the unstable modes towards lower frequency and the simultaneous appearance of higher modes. The latter have been identified as such by additional zeros in the corresponding eigenfunctions [11].
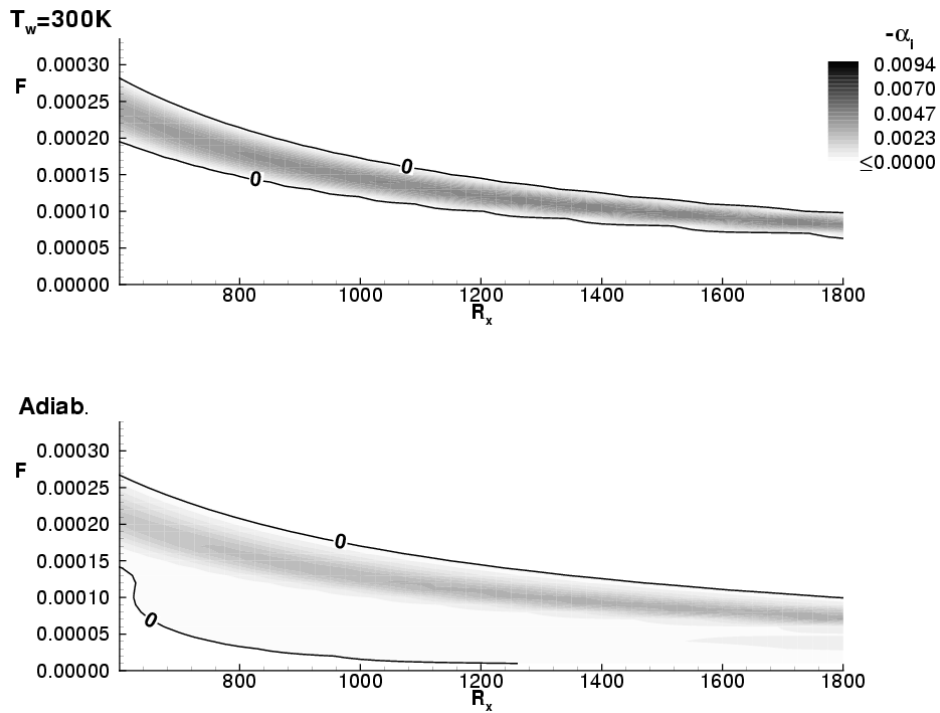
Figure 4: Stability diagrams (amplification rates) of LST for the two flat-plate boundary layers without shock/boundary-layer interaction
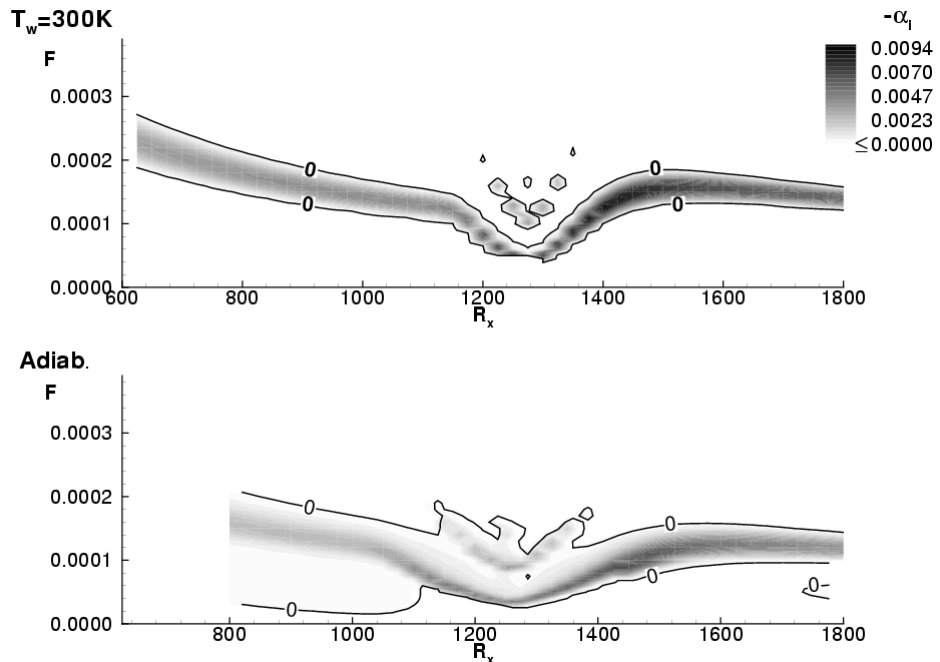
Figure 5: Stability diagrams (amplification rates) of LST for the flat-plate boundary layers with impinging shock

The overall amplification of disturbances at some selected frequencies can be judged from the so-called "N-factors", i.e.

$$N(x) = \ln A(x)/A_0 = \int_{x_0}^{x} -\alpha_i \cdot dx \qquad (8)$$

These are shown first for the isothermal and the adiabatic boundary layers without shock interaction in Fig. 6, then for those with shock/boundary-layer interaction in Fig. 7. In the no-shock case the largest integral amplification occurs for the frequency $F=10^{-4}$. It amounts to $e^{2.5} \approx 12$ which is not exceedingly large what in turn confirms the higher linear stability of the hypersonic boundary layer compared to flows at lower Mach numbers. However, in the case of the shock-induced separation the maximal amplification rises to e^4-$e^6 \approx 55 - 400$ which is quite remarkable. But strong amplification is confined to a narrow range of frequencies, and most of it occurs well after the shock/boundary-layer interaction region because of the increased second-mode instability there, especially for the isothermal wall, cf. Fig. 5. Compared to the no-interaction cases the amplification is much more frequency dependent such that curves for nearby frequencies can exhibit considerable qualitative differences. In the adiabatic case, where the larger separation bubble has been found above, the most amplified frequency remains closer to the one in the no-interaction case. For the following comparisons with DNS we have selected this frequency $F = 10^{-4}$ as a basis.
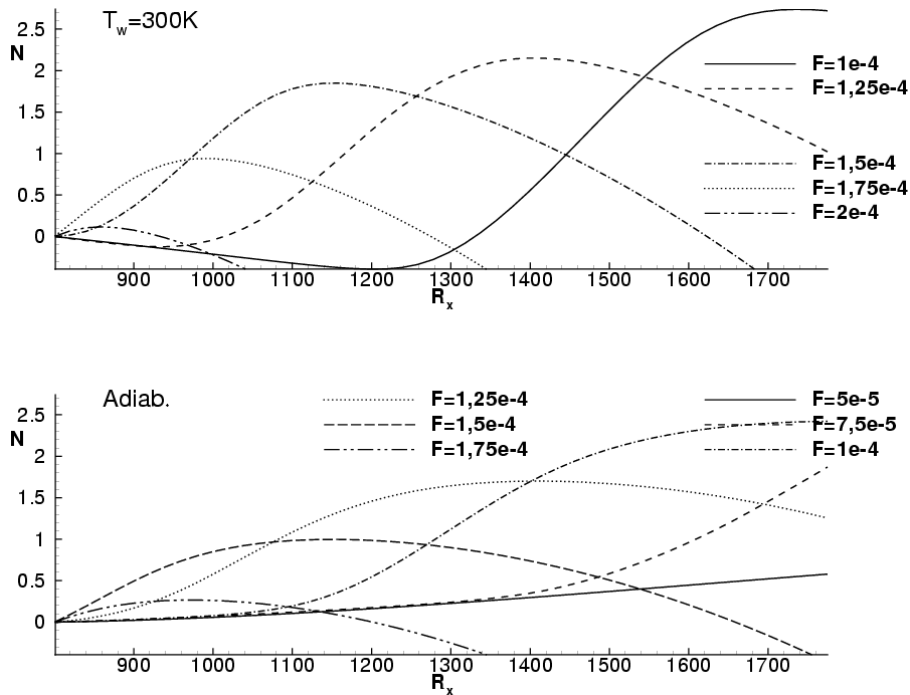
Figure 6: Amplification curves according to linear stability theory for selected frequencies for the flat-plate boundary layer without shock interaction

3.3   Larger-Amplitude Disturbance Behavior

We now turn to the development of larger disturbances yielding non-linear behavior. In the following *(h, k)* represents a mode of the frequency/spanwise-wave-number spectrum, where *h* and *k* denote multiples of the fundamental disturbance frequency and spanwise wave number, respectively. For the cases presented here, a fundamental frequency $F = 10^{-4}$ is chosen and the spanwise wavenumber is set to $\beta = 10.4$.
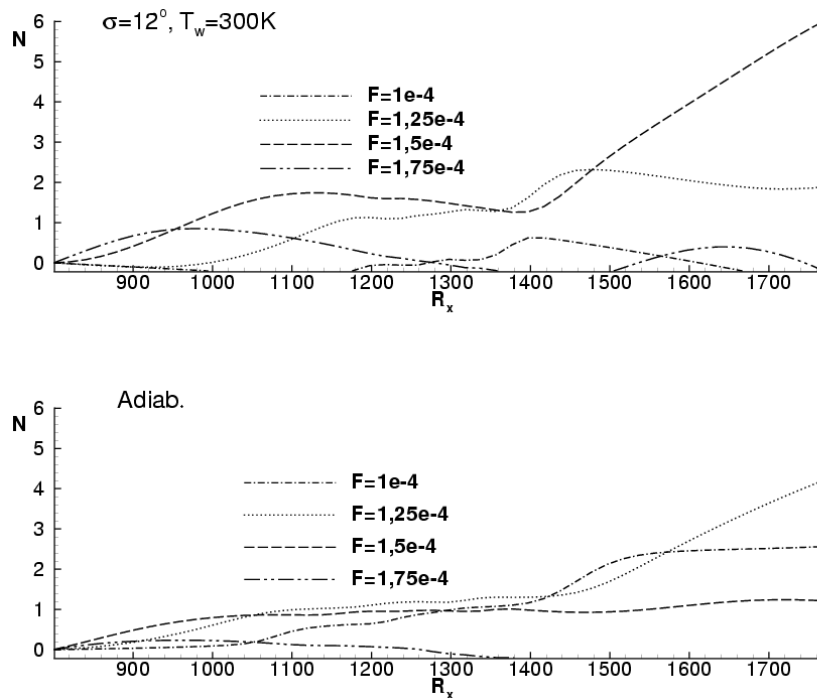
Figure 7: Amplification curves according to linear stability theory for selected frequencies in the cases with shock/boundary-layer interaction

Here, the amplitude of the primary disturbances was set to its maximum possible level (for the present implementation of the disturbance strip at the wall) and non-linear generation of higher harmonic modes as well as non-linear interactions between different modes are to be expected. Three basic scenarios have been simulated for both base flows introduced above. In the following, however, results for the adiabatic wall boundary condition are shown only, because of the higher disturbance amplification for $F = 10^{-4}$ there, compared to the isothermal case (cf. previous section). Basic cases have been selected in order to have some guidance through the many possible non-linear interactions. For a hypersonic boundary layer two such mechanisms are feasible. They consist either of interactions of a large-amplitude two-dimensional second-mode disturbance with small three-dimensional ones or of the direct interaction of a pair of oblique waves. In the literature the former is called "secondary instability" [6] while the latter is called "oblique breakdown" [14]. Two generic cases of secondary instability are considered, one where the three-dimensional secondary disturbance has subharmonic frequency (i.e. $F/2$) with respect to the fundamental and one where both have the same frequency (F).

The downstream development of the temperature fluctuation maxima for these two cases are displayed in Figs. 8 and 9, respectively. They are a characteristic measure for the disturbance amplification A/A_0 [12]. The boundary layer without shock/boundary-layer interaction is always given for reference, its results are marked with symbols in the following figures. By definition, the dominant disturbance for these two scenarios is always the fundamental two-dimensional mode *(1, 0)*. Followed by *(1/2, 1)* or *(1, 1)* in one or the other. A sudden growth of these modes due to a non-linear interaction with the fundamental can only be observed at the very downstream end of the integration domain, i.e. downstream of the shock/boundary-layer interaction zone. Apparently, the two-dimensional disturbance amplitude is not large enough inside the bubble and the conditions for resonance are only met after the additional growth that appears when the primary disturbance enters the instability region behind the bubble (cf. Fig. 7). Compared to the subharmonic case the fundamental three-dimensional disturbance grows earlier but not necessarily to a higher level.

Higher-harmonic modes which are non-linear products of the initial disturbances are also shown. They exhibit the largest differences with respect to the reference cases without shock. The according

steady three-dimensional temperature disturbances of modes *(0, 2)* or *(0, 1)* grow to two orders of magnitude larger values! Without shock/boundary-layer interaction this is clearly not the case. Further down we will look at these steady three-dimensional disturbances in more detail.
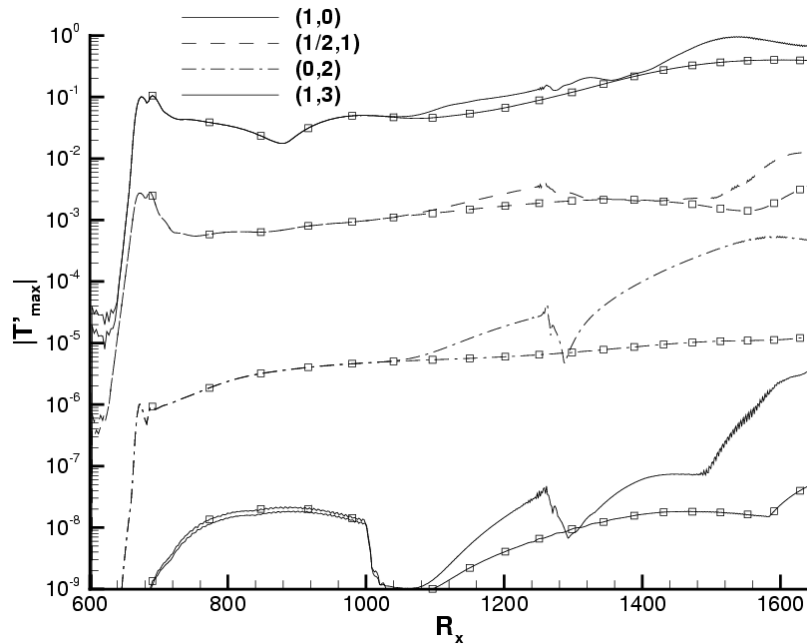
Figure 8: Comparison of amplitude growth of selected modes *(h, k)* for the adiabatic boundary layers with shock/boundary-layer interaction and without (lines with symbols) in the case of subharmonic secondary instability
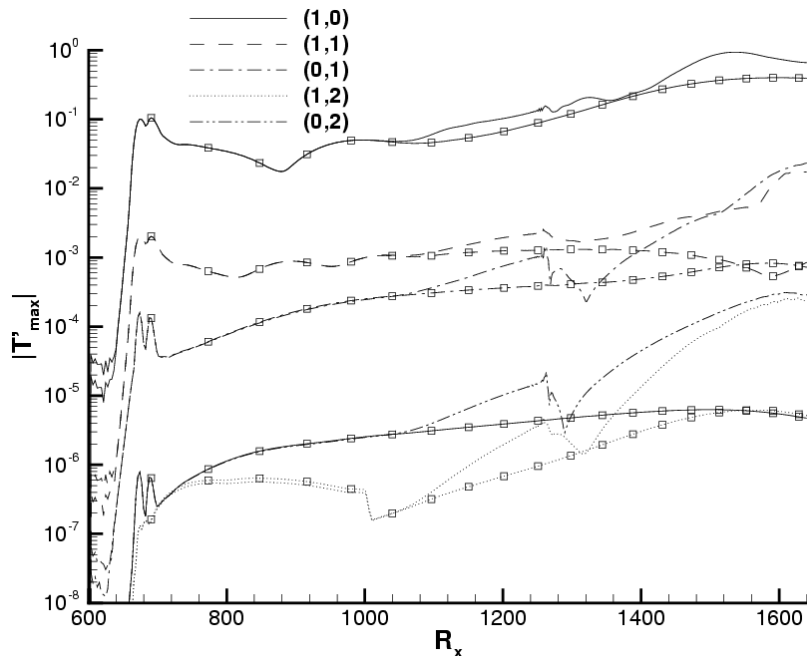
Figure 9: Comparison of amplitude growth of selected modes *(h, k)* for the adiabatic boundary layers with shock/boundary-layer interaction and without (lines with symbols) in the case of fundamental secondary instability

Results of the third non-linear basic scenario, the "oblique breakdown", are displayed in Fig. 10. Now, two oblique waves *(1, 1)* and *(1, -1)* interact with each other. Because of symmetry, it is sufficient to display modes *(h, +k)* i.e. without their symmetric counterparts *(h, -k)*. The fundamental mode *(1, 1)* is represented by a solid line, the directly generated modes *(0, 2)* and *(1, 3)* by dashed and dash-dotted lines, respectively. Again, the reference case without shock is represented by the according lines with squares.
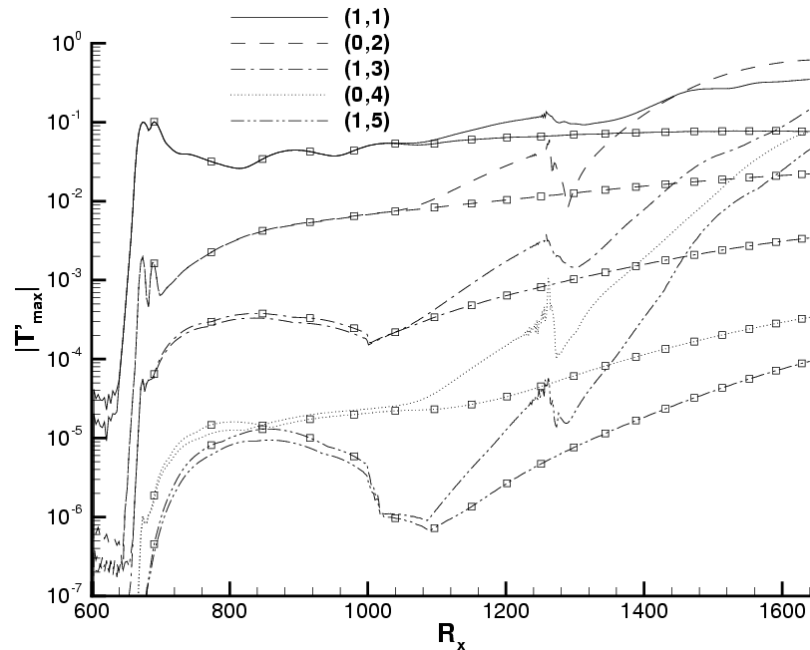
Figure 10: Comparison of amplitude growth of selected modes *(h, k)* for the adiabatic boundary layers with shock/boundary-layer interaction and without (lines with symbols) in the case of oblique wave interaction

It turns out that the disturbance amplitudes in case of shock-wave/boundary-layer interaction strongly exceed the amplitudes of the clean flat-plate flow. Compared to the primary two-dimensional disturbances in the previous cases the primary amplification of the three-dimensional (also a second mode according to Mack) is much weaker now which agrees with linear stability theory (not shown here). Increased amplification of mode *(1, 1)* due to shock/boundary-layer interaction thus becomes much more apparent than before. All higher harmonics grow increasingly faster because they are related to the non-linear products of the primary disturbances. The three-dimensional steady disturbance *(0, 2)* grows by two orders of magnitude, as in the other cases above. Here, however, it grows to larger amplitudes than the primary modes *(1, 1)*. Conversely to further above, mode *(0, 2)* is a characteristic feature of "oblique breakdown" already in the subsonic range [14]. Its initial growth is related to the square of the growth rate of the primary disturbance. Once generated, however, it can overshoot the primary due to a transient growth mechanism often associated with a so-called "lift-up effect" of the boundary layer by the wall-normal velocity disturbance it generates [14]. Here, in the case of the boundary layer without shock this does not occur. Only when shock/boundary-layer interaction is present the three-dimensional steady disturbance grows considerably. Its rather unexpected growth in all cases with shock/boundary-layer interaction investigated here, supports earlier speculations that all this is due to a Görtler instability because of convex streamline curvature in connection with the shock-induced separation bubble at the wall. Indeed, such streamlines can be found in Fig. 1.

The characteristic parameter of the Görtler instability is the Görtler number which is proportional to the wall-curvature radius in the original formulation of the problem [13] and the growth of mode *(0, 2)* in all cases compares well with the concave-convex-concave streamline curvatures in Fig. 1, i.e., there is growth in the separating flow until $R_x \approx 1260$, followed by a decay and additional growth with a maximum

near $R_x \approx 1400$. However, since the streamline curvature changes with distance from the wall and the wall remains flat in the present case a quantitative estimation of the Görtler number remains somewhat ambiguous, despite an effort of Balakumar *et al.* [3] for a compression ramp flow at *Ma=5.37*. Therefore, we tried to find further evidence by looking at the DNS data directly.
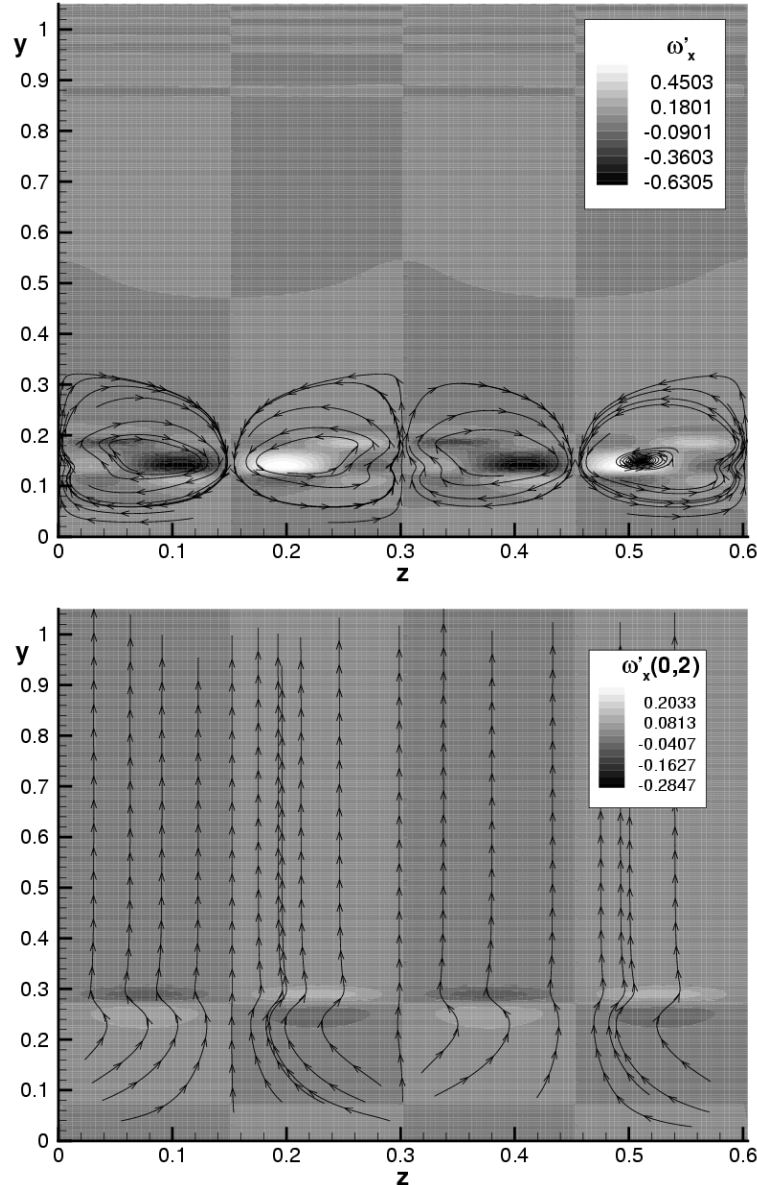
Figure 11: Comparison of secondary flow with streamwise vorticity in a cross-stream cut at R_x=1600 from the oblique breakdown scenario. Boundary layer with shock/boundary-layer interaction (top) and without (bottom).

A comparison of the cross flows downstream of shock/boundary-layer interaction in the oblique case seems to confirm the Görtler hypothesis because of large and clear-cut longitudinal vortices in the top part of the figure which unmistakably don't appear in the absence of the shock interaction. For the second case it is sufficient to consider the streamwise vorticity of mode *(0, 2)* because this one dominates the time-averaged flow. A closer look reveals that the vorticity structure is also completely different in the two cases. With shock/boundary-layer interaction there is a concentration in vortex cores while two weak regions of opposite sign develop at the boundary-layer edge in the case without shock.
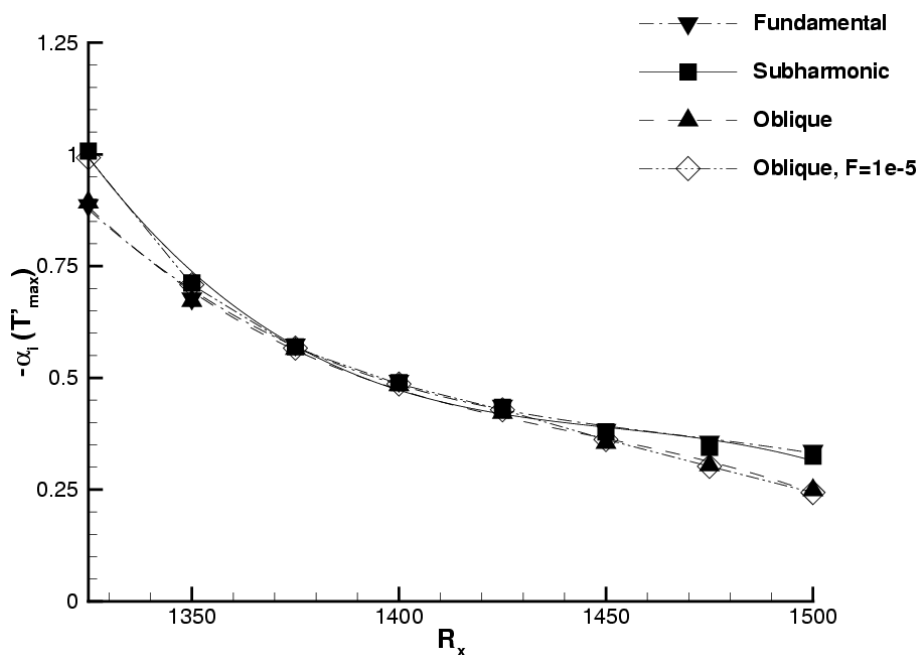
Figure 12: Comparison of amplification rates for mode *(0, 2)* in all investigated non-linear cases

A very convincing support of the above Görtler hypothesis is found when the growth rates of mode *(0, 2)* are extracted from all cases studied and compared to each other. They turn out to be independent of the respective laminar-turbulent transition scenario as well as independent of the primary disturbance frequency. In a pure laminar-turbulent transition scenario, if we select a certain higher harmonic, like the one here, its growth will be completely defined by the growth of the primary disturbances. Since different primary disturbances with different growth rates are necessary to produce the same *(0, 2)* in different scenarios, their growth should be completely different (and frequency dependent). Since this is not the case in Fig. 12, we have found another strong evidence for the contribution of a local instability provided by the base flow alone, like the already mentioned Görtler theory. The role of different non-linear interactions is then restricted to providing different initial conditions (amplitudes) for the ensuing Görtler instability. The growth of these being independent of their amplitude as long as it is not too large.

4.0   CONCLUSIONS

The present investigations have shown that laminar shock/boundary-layer interaction contributes to the primary amplification of small- and medium-amplitude disturbances in a hypersonic boundary layer. The amplitude increase is not too drastic but ratios of *>100* are possible. The primary instability is dominated by increased amplification of the so-called second Mack mode which is two-dimensional. Different non-linear interaction scenarios have confirmed earlier hypotheses stating that a Görtler instability leads to longitudinal vortices in the re-attachment zone of the shock-induced separation bubble. In contrast to such earlier investigations it seems that the growth rates of such vortices has been quantified for the first time here.

ACKNOWLEDGEMENTS

REFERENCES

[1] J.D. Anderson Jr.: Hypersonic and High Temperature Gas Dynamics, McGraw-Hill, 1989.

[2] J.D. Anderson Jr.: Modern Compressible Flow, McGraw-Hill, New York, 1990.

[3] P. Balakumar, H. Zhao, H. Atkins: Stability of hypersonic boundary layers over a compression corner, AIAA 2002-2848.

[4] J. Déléry, J.G. Marvin: Shock-Wave Boundary Layer Interactions, AGARDograph, 280, 1986.

[5] W. Eissler: Numerische Untersuchungen zum laminar-turbulenten Strömungsumschlag in Überschallgrenzschichten, Dissertation, Stuttgart University, 1995.

[6] T: Herbert: Secondary Instability of Boundary Layers, Ann. Rev. Fluid Mech. 20, 487-526, 1988.

[7] L.M. Mack: Boundary layer stability theory, Jet Propulsion Laboratory, Report No. 900-277, 1969.

[8] M. Kloker: A Robust High-Resolution Split-Type Compact FD Scheme for Spatial Direct Numerical Simulation of Boundary-Layer Transition, Applied Scientific Research, Vol. 59, pp. 353-377, 1998.

[9] M. Kloker, U. Konzelmann, H. Fasel: Outflow boundary conditions for spatial Navier-Stokes simulations of transition boundary layers. AIAA Journal 31, pp. 620-628, 1993.

[10] S.K. Lele: Compact Finite Difference Schemes with Spectral-like Resolution, J. Comp. Phys., Vol. 103, pp. 16-42, 1992.

[11] A. Pagella: Numerische Untersuchungen zur transitionellen Stoß-Grenzschicht-Interaktion bei Ma=4,8 und Ma=6, Dissertation, Stuttgart University, 2004.

[12] A. Pagella, U. Rist, S. Wagner: Numerical investigations of small-amplitude disturbances in a boundary layer with impinging shock wave at Ma=4.8, Phys. Fluids, Vol. 14 (7), pp. 2088-2101, 2002.

[13] H. Schlichting, K. Gersten: Boundary-Layer Theory, Springer-Verlag, 8th ed. 2003.

[14] P. Schmid, D. Henningson: Stability and Transition in Shear Flows, Springer-Verlag, Applied Mathematical Sciences Vol. 142, 2001.

[15] K.W. Thompson: Time dependent boundary conditions for hyperbolic systems, J. Comput. Phys., Vol. 68, pp. 1-24, 1987.

[16] F.M. White: Viscous Fluid Flows, 2nd ed., Series in Mechanical Engineering. McGraw-Hill, New York, 1991.